metals

Article

Estimation of the Blast Furnace Hearth State Using an Inverse-Problem-Based Wear Model

Chengbo Zhang [1,2], Binbin Hou [1,2], Lei Shao [1,2,*], Zongshu Zou [1,2] and Henrik Saxén [3]

1 Key Laboratory for Ecological Metallurgy of Multimetallic Mineral (Ministry of Education), Northeastern University, Shenyang 110819, China; zhangcb654@163.com (C.Z.); houbinbin311@163.com (B.H.); zouzs@mail.neu.edu.cn (Z.Z.)
2 School of Metallurgy, Northeastern University, Shenyang 110819, China
3 Process and Systems Engineering Laboratory, Åbo Akademi University, FI-20500 Åbo, Finland; hsaxen@abo.fi
* Correspondence: shaolei@mail.neu.edu.cn

Abstract: An undisturbed and well-controlled hearth state is an essential prerequisite for achieving a long campaign life and low production costs in an ironmaking blast furnace, because hearth wear and hot metal and slag drainage are crucial factors in its operation. With the objective to estimate the hearth state of the refractory of a three-taphole blast furnace, a wear model of the hearth erosion and skull formation was developed. The model is based on thermocouple readings in the hearth lining and solves an inverse heat conduction problem for a series of co-axial vertical slices, where the erosion and skull lines are optimized simultaneously. The model is optimized for fast computation by adopting a novel procedure featuring fixed mesh during the looping calculation. The results revealed that the hearth refractory showed an elephant-foot-shaped profile with excessive erosion in the hearth periphery, indicating that liquid flows are suppressed in the hearth bottom and that the permeability of the core of the deadman is low. These findings were further elaborated and confirmed by a comparison between the estimated hearth state and other key operation variables, including the coke rate, blast kinetic energy, and residual carbon appetite of the hot metal.

Keywords: blast furnace hearth; lining erosion; skull buildup; deadman condition; inverse heat conduction problem

check for updates

Citation: Zhang, C.; Hou, B.; Shao, L.; Zou, Z.; Saxén, H. Estimation of the Blast Furnace Hearth State Using an Inverse-Problem-Based Wear Model. *Metals* **2022**, *12*, 1302. https://doi.org/10.3390/met12081302

Academic Editors: Hong Yong Sohn and Srecko Stopic

Received: 24 May 2022
Accepted: 29 July 2022
Published: 3 August 2022

1. Introduction

The lowest part, the hearth, is a crucial region of the blast furnace (BF), which is the dominant industrial unit for the production of liquid iron ("hot metal"), which is the raw material for primary steelmaking [1,2]. It is widely recognized that the state of the hearth plays a crucial role in the performance of the BF, and that an undisturbed and well-controlled hearth state is an essential prerequisite for achieving an efficient operation, a low energy consumption, and a long campaign life of the BF [3–7]. Nevertheless, it is of considerable difficulty, if not impossible, to directly measure the hearth state of an operating BF because of the extremely harsh environment with high temperatures and the presence of chemically aggressive molten phases. In order to shed light on the prevailing state of the hearth, BF operators usually resort to an estimation based on indirect measurements, the most important of them being the temperatures measured by thermocouples (TCs) embedded in the hearth lining.

The campaign life of the BF mainly depends on the service life of the hearth lining, which is associated with the performance of the refractories [8]. There are mainly two types of hearth designs for BF, including carbonaceous bricks and oxide bricks (ceramic cup) in combination with carbonaceous bricks. The carbonaceous bricks have high thermal conductivity and cooling capacity and are expected to "freeze" hot metal on their hot face, creating a build-up ("skull") layer to protect the remaining lining. However, the carbonaceous bricks have a low degree of resistance to the erosion of hot metal and molten slag. If the skull is absent, carbon-unsaturated hot metal may consume the carbonaceous bricks, causing hearth wear. The oxide bricks with low thermal conductivity and high erosion resistance are capable of slowing down the hearth wear. Nevertheless, the ceramic cup will disappear as a result of erosion, and the protection will disappear as well. In a way, the protection of the oxide bricks is similar to the skull layer. The properties of different carbonaceous and oxide bricks are listed in Tables 1 and 2, respectively. Although there are differences in the two hearth designs, their technical goals are the same: the refractory materials cooperate with the cooling system to make the 1150 °C isotherm, below which carbon-saturated iron cannot exist in liquid form, and move toward the center of the hearth as much as possible. The hearth lining erosion and skull buildup are commonly regarded as the most informative indicators of the hearth state [9]. With knowledge about these, timely and suitable control and maintenance actions can be taken to avoid an unfavorable state characterized by either severe erosion of lining refractories or excessive growth of skull layers. The former may eventually lead to an outbreak of hearth liquids with potentially catastrophic consequences, while the latter is also detrimental as it reduces the effective hearth volume and thus lowers possibilities of maintaining a high production rate. Further, it influences the internal flow field of the liquids that may affect the state (e.g., carburization) of the hot metal.

Table 1. Properties of different carbonaceous bricks in hearth lining, data were compiled from [8].

Properties		Unit	Microporous	Super Micropore	Graphite	Carbon
Bulk density		g/cm^3	1.62	1.72	1.62	1.56
Porosity		%	16	16	23	20
Modulus of rupture		Mpa	13	18	10	10
Crushing strength		Mpa	45	55	20	34
Thermal conductivity	400 °C	W/(m·K)	16	20	160	18
	1000 °C	W/(m·K)	3.5	3.5	3.1	3.5

Table 2. Properties of different oxide bricks in hearth lining, data were compiled from [8].

Properties	Unit	Mullite	Corundum-Mullite	Corundum-SiAlON Bonded	Corundum-Chrome Oxide
Al_2O_3 content	%	74	85	70	87
Bulk density	g/cm^3	2.55	3.05	3.15	3.15
Permanent linear change at 1500 °C	%	0.5	0.1	0.4	0.4
Thermal conductivity at 1000 °C	W/(m·K)	2.2	3.2	3.5	3.5

Over the years, numerous efforts have been made to develop wear models that can be used to offer an overall picture of the hearth internal geometry particularly with respect to lining and skull profiles [9–15]. Such wear models build on the solution of inverse heat conduction problems, where the deviations between thermocouple readings and temperatures estimated by a mathematical model at the same points are minimized by iteratively altering the location and shape of the inner profile. Commonly, the inner profile is described as the 1150 °C isotherm. Different models of this kind, in both one and two dimensions, have been developed and implemented in industrial BFs, serving as an indispensable monitoring/diagnosis tool to aid in the hearth management [9,12,14,15]. More recently, a considerable expansion of the traditional wear model for estimating the hearth internal geometry into three dimensions using a multi-physics platform was presented [14]. Even though this approach is associated with a heavy computational burden, it was demonstrated to be versatile and capable of providing additional information about the hearth state, such as thermal stresses and deformation of the hearth lining and steel shell.

In practice, most changes of the lining state are triggered by changes in the conditions inside the hearth, which, in turn, are intimately linked to the deadman condition that strongly affects the flow patterns and outflow behavior of molten slag and hot metal [16–20]. Therefore, some attempts were made in the past to correlate the results from the wear model with potential BF variables that may trigger, or reflect, changes in the hearth state in order to gain a better understanding of the complex system at hand. Torrkulla et al. [10] estimated the six-year evolution of the available hearth volumes of twin single-taphole BFs (i.e., BF A and BF B, approximately 1000 m^3) on the basis of a wear model, comparing the findings with changes in the measured slag delay, which expresses the time elapsed between the beginning of a tap and the moment when slag outflow starts. The comparisons showed no discernible correlation between the hearth volume and the slag delay for BF A, while for BF B, a strong negative correlation was observed. The authors argued that the correlation is attributed to a (partially) floating deadman during the campaign of BF B. For BF A, the deadman (with a low voidage) was less active and extended to the hearth bottom, eventually resulting in a large scab, as found in the hearth at a mid-campaign repair. On the basis of measured tap duration and slag delay, the authors also carried out an estimation of the deadman voidage using a (simplified) model originally reported by Nightingale and Tanzil [21]. It has been revealed that a decrease in the deadman voidage generally corresponds to an increase in the amount of skull formed on the hot face of the remaining lining.

A generic wear model optimized for fast computation, and thus industrial application has been presented in a previous paper [11], where special emphasis was put on outlining the underlying principles of the model and introducing the measures for yielding a well-conditioned numerical problem. Some examples of the estimated lining and skull profiles featuring three-dimensional (3D) representations were also presented. The wear model was later implemented in a three-taphole BF, and its results have been used by the BF operators on a daily basis to aid in the hearth state diagnosis and management. With the intent to further explore the complex hearth state, a thorough examination of long-term evolutions of the hearth quantities estimated by the wear model is described in the current paper. Attempts are also made to interpret the hearth state by studying correlations between some of its results and other relevant BF variables, including the coke rate, blast kinetic energy, and residual carbon appetite of tapped hot metal.

2. The Blast Furnace Hearth and Wear Model

2.1. The Blast Furnace and Its Hearth

The generic wear model was implemented in the control system of a 2500 m^3 BF, which was blown in on 26 June 2012 and has a target campaign life of 15 years. Figure 1a shows a sketch and some key design parameters of the BF.

As depicted in Figure 1b, the BF under consideration has 30 tuyeres and 3 tapholes (labeled TH1, TH2, and TH3). The dashed lines denoted by S1–S8 in Figure 1b refer to eight vertical sections, where a sufficient set of N-type TCs (i.e., typically 10–13 pairs) are embedded in the lining of the hearth. A detailed 3D structure of the hearth is provided in Figure 1c, where it is seen that the hearth is constructed of different refractories, including three types of carbon bricks (I: microporous carbon brick (MCB), II: super-micropore carbon brick (SMCB), III: graphite carbon brick (GCB)) and a complete ceramic cup comprising two types of mullite bricks (IV: corundum-mullite brick (CMB), V: mullite brick (MB)). In the present study, the thermal conductivity of skull in the hearth is given as a commonly adopted fixed value of 2.0 W/(m·K) [12,15,22] in the absence of reliable means to quantify this parameter.

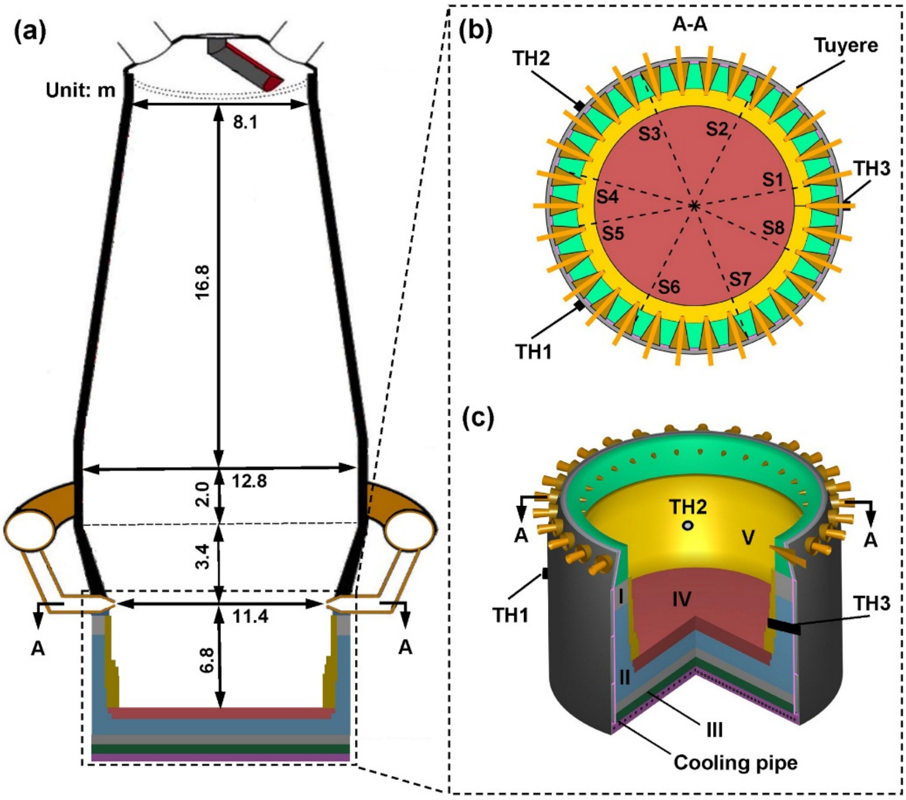

Figure 1. Schematic illustration of the blast furnace and its hearth: (**a**) sketch of the blast furnace with some key design parameters, (**b**) top-view from the horizontal cross-section at the tuyere level (i.e., A-A), and (**c**) detailed structure of the hearth in three dimensions.

2.2. Brief Description of the Wear Model

The wear model has been described thoroughly in an earlier paper by the present authors [9]. For the sake of brevity, therefore, only a brief presentation and the governing equations of the model are outlined in this subsection. The reader is referred to Zhang et al. [9] and Brännbacka and Saxén [10] for more detailed information about the model as well as its validation.

2.2.1. Key Treatments

Numerical calculations acting as the basis of the wear model are performed in two-dimensional (2D) domains corresponding to a series of co-axial vertical slices, where the erosion and skull lines are optimized simultaneously based on the solution of a transformed inverse heat conduction problem. In order to facilitate mathematical implementation, the erosion and skull lines are characterized using a method of direction vectors. With the intent to overcome the drawbacks caused by generating a new computational mesh in every loop of calculation, a novel procedure featuring fixed mesh during looping calculation is adopted. It should, moreover, be pointed out that individual calculations in the 2D domains usually lead to slightly different positions of erosion and skull lines at the central axis. For this, a special subroutine is applied to obtain unique positions at the central axis. After this, all the 2D results are aggregated into smooth 3D profiles using a cubic spline interpolation scheme. These key treatments are schematically illustrated in Figure 2, where it is indicated that the 2D computational domains are chosen on the basis of S1–S8 in the hearth (cf. Figure 1b).

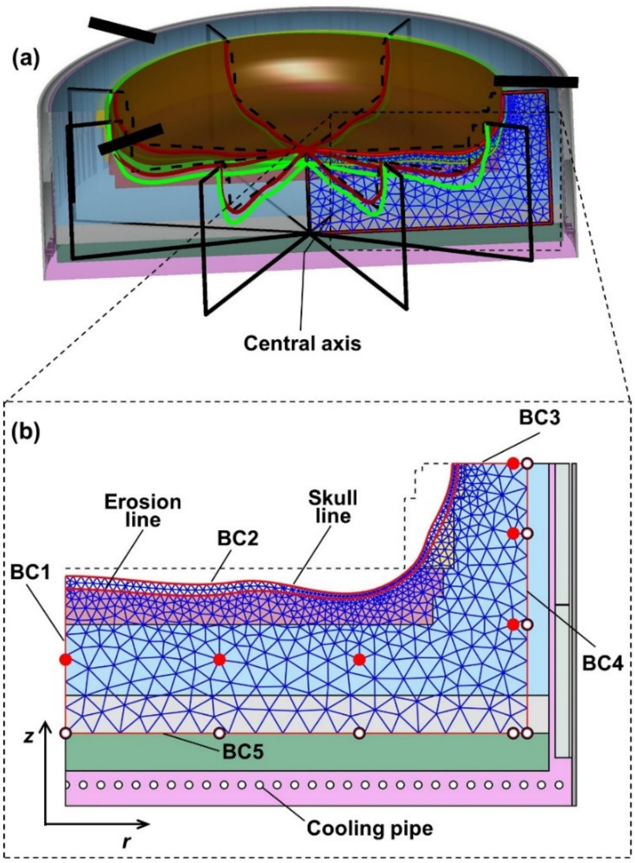

Figure 2. Schematic illustration of the key treatments in the present wear model: (**a**) aggregation of two-dimensional results into a three-dimensional representation (with the tapholes denoted by black bars), (**b**) computational mesh and boundary conditions of a certain vertical section.

2.2.2. Governing Equations

The red dots in Figure 2b represent the reference TCs, of which the calculated temperatures are retrieved when the temperature (T) distribution in each computational domain is determined by solving the following partial differential equation in two spatial coordinates, r and z (cf. the lower panel of Figure 2).

$$\frac{1}{r}\frac{\partial}{\partial r}\left(r\lambda\frac{\partial T}{\partial r}\right)+\frac{\partial}{\partial z}\left(\lambda\frac{\partial T}{\partial z}\right)=0 \tag{1}$$

where λ is the thermal conductivity of the solid materials including the hearth lining refractories as well as the skull layer limited by the erosion and skull lines.

In each of the computational domains, the finite element method is applied to determine the temperature distribution, while the Levenberg–Marquardt algorithm is utilized to tackle the inverse heat conduction problem, for which the objective function, E, is written as

$$E=\sum_{i=1}^{M}\left(T_i^{\mathrm{c}}-T_i^{\mathrm{m}}\right)^2+\gamma\sum_{j=1}^{N}\left(\alpha_j-\tilde{\alpha}_j\right)^2 \tag{2}$$

where the superscripts ‘c’ and ‘m’ stand for the calculated and measured variables (i.e., temperatures of the M reference TCs), respectively. The second term on the right-hand side is a scaled regularization used to avoid physically unlikely bending of the internal profile.

3. Results and Discussion

3.1. Graphical User Interface-Based Platform

In order to facilitate its daily use by the BF operators, extensive programming has been carried out in order to convert the hearth wear model into a graphical user interface-based platform, which is a standalone system consisting of four parts accounting for parameters setup, data plausibility checks and filtering, calculation execution, as well as results' visualization and export. The interface of results' visualization and export offers the user freedom to examine the results in detail. A variety of quantities, such as temperature distribution within the hearth, skull and erosion profiles (in two and three dimensions), volumes of skull and remaining hearth lining, available hearth volume, as well as heat losses through the hearth bottom and sidewalls, can be readily accessed. If needed, illustrative graphs or tables of data can also be exported and stored for later use. A special algorithm was developed and applied in the wear model with the aim to separately compute the volumes of skull formed on the hearth bottom as well as the one on the sidewalls.

For the purpose of demonstration, Figure 3 provides a window of the most frequently used interface for results' visualization and export. The window shows the estimated 2D skull and erosion profiles in the eight vertical sections (cf. S1–S8 in Figure 1b) for a selected date. The dashed lines in each of the eight sub-figures depict the shape of the initial ceramic cup. The red dots represent the TCs, of which the readings (in °C) are also presented. It is clearly seen in Figure 3 that the extent to which the ceramic cup is eroded differs greatly among the vertical sections distributed along the angular direction of the hearth, with a considerable "gutter" for iron flow formed at the outer part of the hearth bottom in the vicinity of the two tapholes (TH2 and TH3) located close to each other.

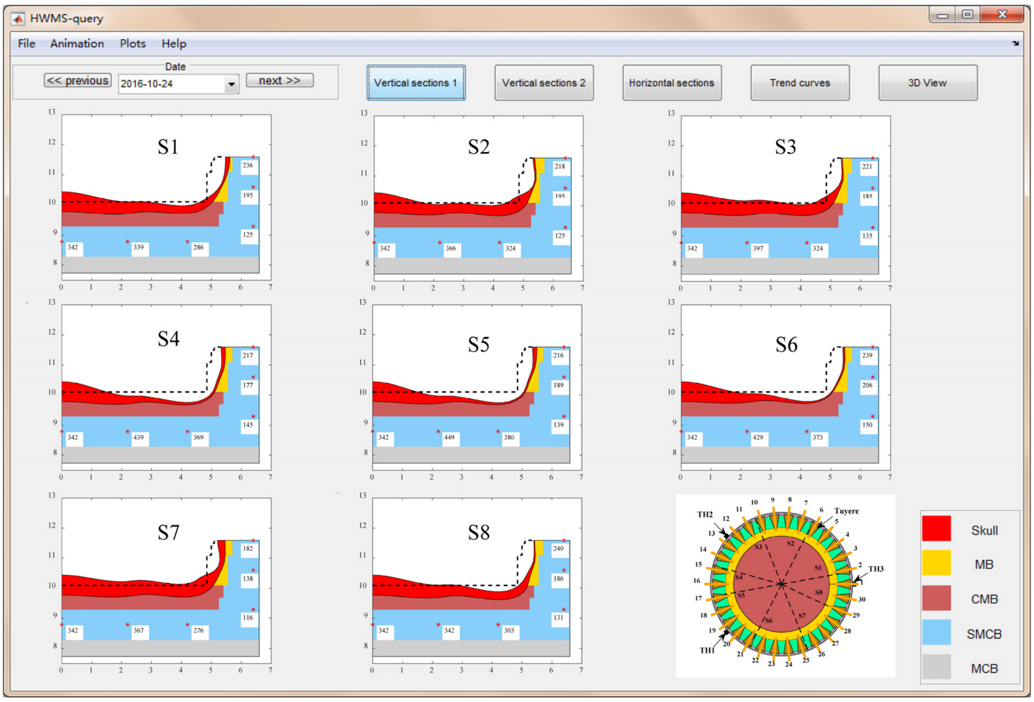

Figure 3. Skull and erosion profiles in the eight vertical sections (cf. S1–S8 in Figure 1b) of the blast furnace hearth for a selected date.

Using the interpolation scheme, the 2D results in the eight vertical sections can be aggregated into 3D profiles, as illustrated in Figure 4. The user can make a comparison of the estimations for totally three selected dates by visualizing them in three columns. In each column, a 3D hearth internal geometry that can be zoomed and rotated arbitrarily is presented in the upper panel, where the colors express the thickness of the skull layer and range from blue (skulled) to red (eroded). A navigating rod (cf. the bold dashed line with a dot) above the 3D internal geometry indicates the selected vertical cross section and the corresponding skull and erosion profiles are shown in the lower panel. The user can change the circumferential angle of the navigating rod with respect to the centerline of TH3 by altering the input in the "Angle" textbox at the top of each column.

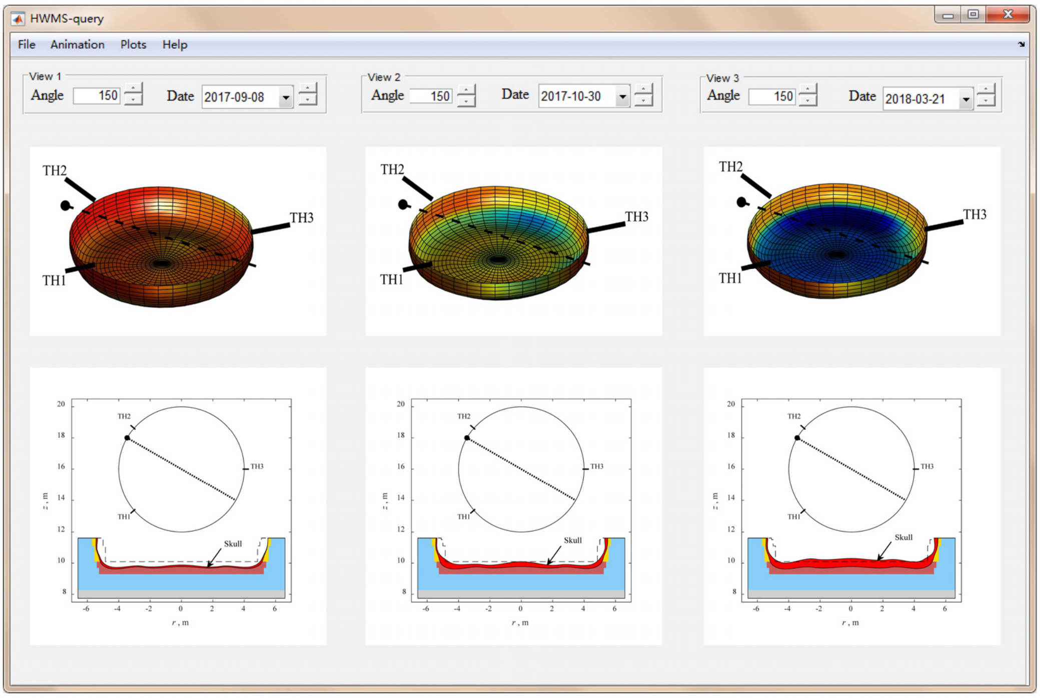

Figure 4. Three-dimensional representations of the internal geometry of the blast furnace hearth for three selected dates.

3.2. Estimation of the Hearth State

The wear model was applied to daily mean values of hearth lining TC readings spanning roughly 2500 days of operation since the blow-in of the industrial BF in 2012. Figure 5 shows the evolutions of some central results of the model for the period, i.e., the volumes of eroded lining (upper panel), bottom skull (solid line, lower panel), as well as sidewall skull (dashed line, lower panel) within the hearth region considered by the model. The latter variables were slightly filtered to suppress short-term variations that were not considered to reflect true changes in the hearth state.

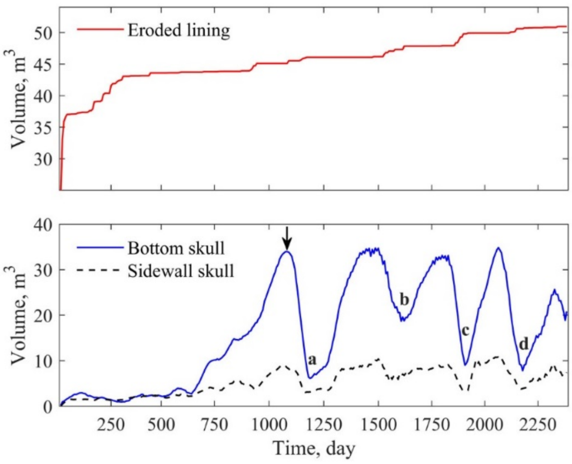

Figure 5. Evolutions of volumes of eroded lining (**upper** panel), bottom skull (solid line, **lower** panel), and sidewall skull (dashed line, **lower** panel) within the hearth region considered by the wear model.

During the first year of the BF campaign, the low-conducting ceramic cup with an average initial thickness of approximately 0.75 m was mostly eroded at a rather rapid speed (cf. upper panel), and the volumes of the bottom skull and sidewall skull are fairly limited (cf. lower panel of Figure 5). Onward from this early stage characterized by rapid lining erosion, the hearth lining is seen to experience a comparatively slow long-term erosion, but the skull volumes increase substantially. More interestingly, after strong growth for days 600–1100 of the campaign, the volumes vary in a cyclical manner that shows a strong similarity to the findings from other BFs [9,15,23,24]. However, the cyclic variation is not entirely periodic, but recurs with a period of 9 to 18 months, which is substantially longer than the period (1–6 months) observed in other furnaces.

It is also revealed in Figure 5 that the erosion of the hearth lining primarily takes place at the major troughs of the skull volumes, labeled a, b, c, and d in the lower panel. In order to analyze the erosion profile further, both the horizontal (left column) and vertical (right column) cross sections of the estimated hearth internal geometry at the four major troughs are depicted in Figure 6. The vertical cross section in the right panel row is taken along the bold dashed line indicated on the left, where the horizontal cross section is taken along the bold dashed line on the right. Moreover, 2D inner profiles of residual hearth refractories are extracted from the vertical cross sections and compared in the lower panel of Figure 6.

It can be seen that, at the four extreme points, the refractories in the center of the hearth bottom are worn to a lesser extent, while lining erosion occurs in the sidewalls and hearth periphery region. Thus, it may be concluded that the BF hearth investigated here shows an elephant-foot-shaped wear profile, which is often attributed to a circumferential iron flow emerging when the permeability in the center of the deadman deteriorates. The lower panel of Figure 5 substantiates this argument, as it is clearly shown that the volume of the bottom skull (ranging between 3 m^3 and 35 m^3) is much larger than that of the sidewall skull (ranging between 3 m^3 and 10 m^3), indicating a suppressed iron flow in the bottom of the hearth as a result of a low permeability in the core of the deadman. Another conclusion that can be drawn is that the general skulling and erosion processes first occur at the sidewall and then spread to the hearth bottom. This is seen if the evolutions of the bottom and sidewall skulls are normalized to facilitate a comparison. Figure 7 shows the normalized skull volumes, expressed as the estimated skull volume divided by the maximum one. The figure reveals that most peaks and troughs occur a few days earlier for the sidewall than for the bottom, which is in agreement with earlier findings based on hearth wear models [9,10,15]. It is thus indicated that there is an internal competition of central and peripheral flows of hot metal. When the furnace progresses from a skulled state to a state with little skull, the sidewall skull is first eroded/dissolved, followed by an erosion/dissolution of the bottom skull. The latter, in turn, gives rise to lower hot metal flow rates at the sidewall, which leads to wall skulling, followed by bottom skulling. As elaborated in [9,15], these patterns may also be associated with a cyclic deadman motion (i.e., partially floating vs. sitting).

The deadman permeability is known to be connected to the consumption rate of coke debris and/or unburned coal fines that may occupy the void space of the coke bed [25,26]. In order to improve the deadman permeability, increasing the coke rate (and correspondingly decreasing the PCI rate) and adopting a higher blast flow rate (to increase the blast kinetic energy) are usually taken as key measures in practice to accelerate the consumption process. A higher kinetic energy of the blast causes the gas to penetrate deeper into the coke bed, which may enhance the contact between the gas and fines and increase their consumption. However, an excessive increase in the blast velocity should be avoided, as it in turn may create more fines due to the grinding and swirling motion of coke particles in the raceways. It is thus implied that both the coke rate and blast kinetic energy may play a crucial role for the formation of the bottom skull because liquid flows in the hearth bottom can be enhanced with an improved deadman permeability. Figure 8 depicts the evolutions in the coke rate, blast kinetic energy, as well as bottom skull volume during the period starting from the first spike (denoted by the downward arrow) in the lower panel of Figure 5. It can be observed in Figure 8 that the bottom skull volume shows a negative correlation with the coke rate and blast kinetic energy; the bottom skull volume is reduced when the coke rate and/or blast kinetic energy is increased.

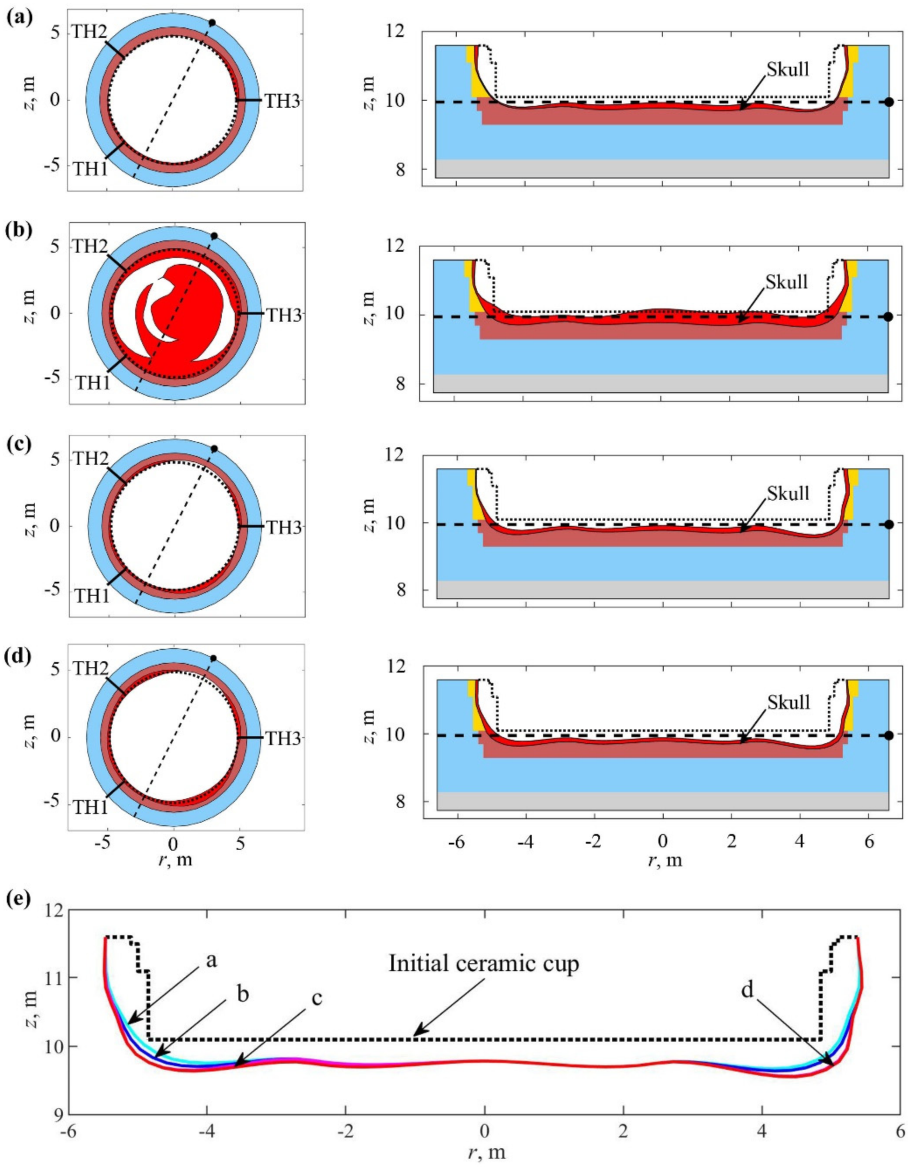

Figure 6. (**a**–**d**) Horizontal (**left** column) and vertical (**right** column) cross sections of the estimated hearth internal geometry for four selected dates corresponding to the major troughs labeled a, b, c, and d in Figure 5, respectively, (**e**) two-dimensional inner profiles of residual hearth refractories for four selected dates corresponding to the major troughs labeled a, b, c, and d in Figure 5.

In the literature [23,24,27], the deadman condition has also been assessed using the residual carbon appetite of tapped hot metal, which is expressed as

$$\Delta Y_{\mathrm{C}} = Y_{\mathrm{sat}} - Y_{\mathrm{C}} \tag{3}$$

where Y_{sat} and Y_{C} are the mass fraction of carbon at saturation and the measured mass fraction of carbon in the tapped hot metal, respectively.

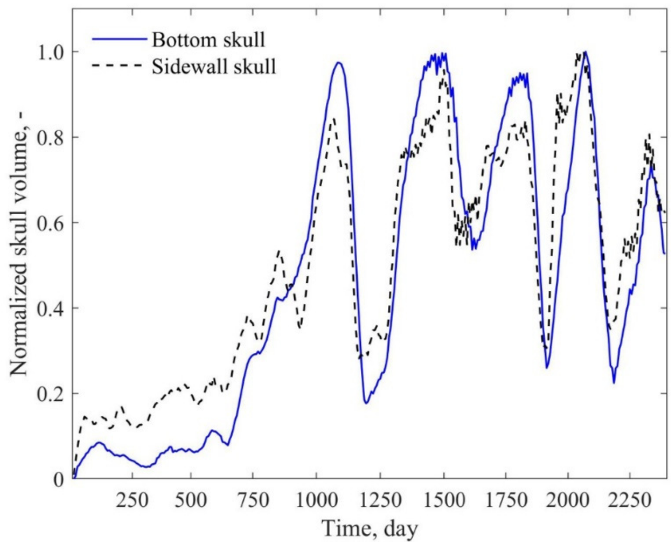

Figure 7. Evolutions of the normalized volumes of bottom skull (solid line) and sidewall (dashed line) skull.

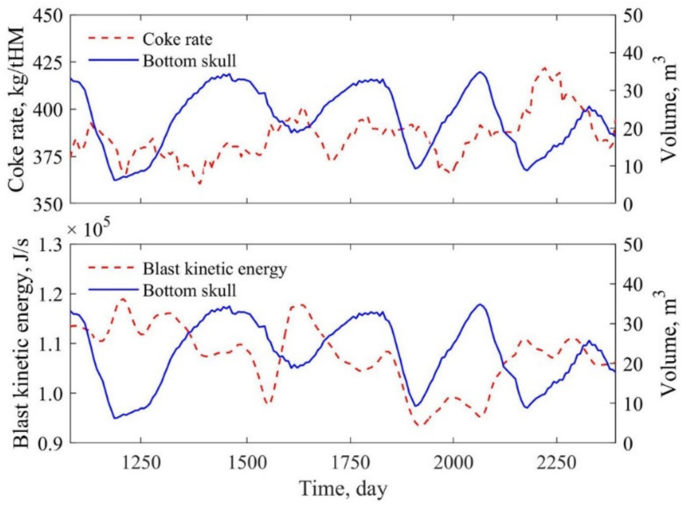

Figure 8. Evolutions of volume of the bottom skull (solid line) within the hearth, coke rate (dashed line, **upper** panel), and blast kinetic energy (dashed line, **lower** panel) of the blast furnace.

For the same period of time as in Figure 8, the evolutions in the coke rate (upper panel) and residual carbon appetite (lower panel) of the BF are illustrated in Figure 9, where it can be seen that a high coke rate generally corresponds to a low residual carbon appetite. This observation further validates the aforementioned argument concerning how the coke rate affects deadman permeability, and thus liquid flow patterns within the hearth; the residence time of hot metal in the hearth is prolonged as the deadman permeability is improved by increasing the coke rate, eventually leading to a more complete carbonization of hot metal and a lower residual carbon appetite. This explanation is also supported by the findings of a previous study [27] on hot metal carbonization in a BF hearth, where the center of a sitting deadman with less permeable core was found to mimic in the state of the hearth of a 1000 m^3 single-taphole BF [28]. At the hearth periphery, nevertheless, the deadman floats slightly and has a higher voidage.

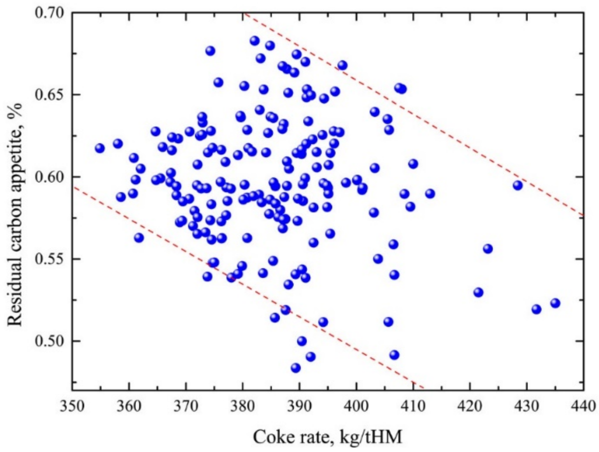

Figure 9. Comparisons between the coke rate and residual carbon appetite of tapped hot metal from the blast furnace.

In the single-taphole BF referred to above, the carbon and sulfur contents of the hot metal exhibited a marked negative correlation. This is because the desulphurization and carbonization of hot metal in the hearth are obstructed when the deadman permeability deteriorates, especially in its center zone. For the large BF considered in the present study, a similar correlation was obtained, as demonstrated in Figure 10. It is thus believed that the behavior of the deadman in the hearth investigated in the present study bears a strong resemblance with what has been reported earlier [28].

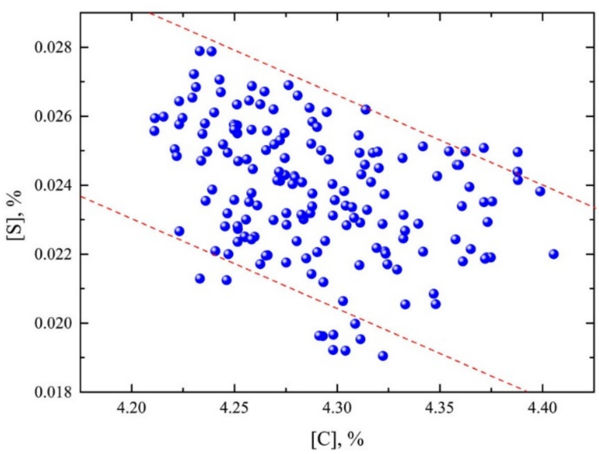

Figure 10. Comparisons between carbon and sulfur contents of tapped hot metal from the blast furnace.

4. Conclusions and Future Work

In this paper, the hearth state of a three-taphole BF was estimated using an inverse-problem-based wear model. The wear model was developed into a graphical user interface-based platform to facilitate its daily use by the BF operators. Long-term evolutions of the estimated volumes of the eroded lining, bottom skull, as well as sidewall skull were examined thoroughly for the reference BF. It was demonstrated that the early stage of the BF campaign is characterized by rapid lining erosion and limited skull formation. After this, the hearth lining experiences a slow and long erosion process, while the skull volume varies in a cyclic manner that is not entirely periodic, but with peaks and troughs recurring within a period of 9–18 months. It was also revealed that the hearth was worn to yield an elephant-foot-shaped profile with excessive erosion in the hearth periphery, indicating that the iron flows are suppressed in the hearth bottom, most likely due to a low permeability of the core of the deadman. The proposed deadman condition was further elaborated and explained by a detailed comparison between the estimated hearth quantities and BF variables, including the coke rate, blast kinetic energy, and residual carbon appetite of the hot metal. Like in other BFs, a marked negative correlation was found between the carbon and sulfur contents of the hot metal, mainly because the desulphurization and carbonization of hot metal in the BF hearth are obstructed when the deadman permeability deteriorates, especially in its center zone.

In forthcoming work, the wear model will be implemented in other industrial BFs, where the conditions regarding raw materials, hearth lining structure, as well as operating principles are different from that considered in the current work. As the underlying reasons and the observed behavior of the BF hearth still remain partly unexplored, future interpretation and analysis of the complex black-box system will be undertaken with the aid of simulations based on computational fluid dynamics and big data techniques.

Author Contributions: Conceptualization, L.S. and H.S.; Data curation, C.Z. and B.H.; Formal analysis, C.Z. and L.S.; funding acquisition, L.S. and Z.Z.; Investigation, C.Z.; Methodology, L.S. and C.Z.; Project administration, L.S.; Resources, L.S.; Software, Z.Z.; Supervision, L.S.; Validation, L.S.; Visualization, C.Z.; writing—original draft preparation, C.Z. and L.S.; writing—review and editing, L.S., Z.Z. and H.S. All authors have read and agreed to the published version of the manuscript.

Funding: This research was partially funded by the National Natural Science Foundation of China (grant no. 51604068) and the National Key R&D Program of China (grant no. 2021YFB1715500).

Data Availability Statement: Not applicable.

Conflicts of Interest: The authors declare no conflict of interest.

References

1. Jiao, K.; Zhang, J.; Liu, Z.; Deng, Y.; Chen, C. Cooling phenomena in blast furnace hearth. *J. Iron Steel Res. Int.* **2018**, *25*, 1010–1016. [CrossRef]
2. Pei, M.; Petäjäniemi, M.; Regnell, A.; Wijk, O. Toward a fossil free future with HYBRIT: Development of iron and steelmaking technology in Sweden and Finland. *Metals* **2020**, *10*, 972. [CrossRef]
3. Guo, B.; Yu, A.; Zulli, P.; Maldonado, D. CFD modeling and analysis of the flow, heat transfer and mass transfer in a blast furnace hearth. *Steel Res. Int.* **2011**, *82*, 579–586. [CrossRef]
4. Andreev, K.; Louwerse, G.; Peeters, T.; van der Stel, J. Blast furnace campaign extension by fundamental understanding of hearth processes. *Ironmak. Steelmak.* **2017**, *44*, 81–91. [CrossRef]
5. Shao, L.; Xiao, Q.; Zhang, C.; Zou, Z.; Saxén, H. Dead-man behavior in the blast furnace hearth—A brief review. *Processes* **2020**, *8*, 1335. [CrossRef]
6. Lüngen, H.; Schmöle, P. Comparison of blast furnace operation modes in the world. *Steel Res. Int.* **2020**, *91*, 2000182. [CrossRef]
7. Dong, X.; Zulli, P. Prediction of blast furnace hearth condition: Part I—A steady state simulation of hearth condition during normal operation. *Ironmak. Steelmak.* **2020**, *47*, 307–315. [CrossRef]
8. Biswas, S.; Sarkar, D. *Introduction to Refractories for Iron- and Steelmaking*; Springer International Publishing: Cham, Switzerland, 2020; pp. 165–195.
9. Brännbacka, J.; Saxén, H. Model for fast computation of blast furnace hearth erosion and buildup profiles. *Ind. Eng. Chem. Res.* **2008**, *47*, 7793–7801. [CrossRef]
10. Torrkulla, J.; Saxén, H. Model of the state of the blast furnace hearth. *ISIJ Int.* **2000**, *40*, 438–447. [CrossRef]
11. Zhang, C.; Zhao, C.; Shao, L.; Saxen, H.; Qu, Y.; Zou, Z. Numerical estimation of hearth internal geometry of an industrial blast furnace. *Steel Res. Int.* **2022**, *93*, 2100364. [CrossRef]
12. Zagaria, M.; Dimastromatteo, V.; Colla, V. Monitoring erosion and skull profile in blast furnace hearth. *Ironmak. Steelmak.* **2010**, *37*, 229–234. [CrossRef]
13. Zhao, H.; Huo, S.; Cheng, S. Study on the early warning mechanism for the security of blast furnace hearths. *Int. J. Miner. Metall. Mater.* **2013**, *20*, 345–353. [CrossRef]
14. Kaymak, Y.; Bartusch, H.; Hauck, T.; Mernitz, J.; Rausch, H.; Lin, R. Multiphysics model of the hearth lining state. *Steel Res. Int.* **2020**, *91*, 2000055. [CrossRef]
15. Helle, M.; Saxén, H.; de Graaff, B.; van der Bent, C. Wear-model-based analysis of the state of blast furnace hearth. *Metall. Mater. Trans. B* **2022**, *53*, 594–603. [CrossRef]
16. Shao, L.; Saxén, H. Numerical prediction of iron flow and bottom erosion in the blast furnace hearth. *Steel Res. Int.* **2012**, *83*, 878–885. [CrossRef]
17. Li, Y.; Cheng, S.; Zhang, P.; Zhou, S. Sensitive influence of floating state of blast furnace deadman on molten iron flow and hearth erosion. *ISIJ Int.* **2015**, *55*, 2332–2341. [CrossRef]

18. Liu, W.; Shao, L.; Saxén, H. Experimental model study of liquid-liquid and liquid-gas interfaces during blast furnace hearth drainage. *Metals* **2020**, *10*, 496. [CrossRef]
19. Bambauer, F.; Wirtz, S.; Scherer, V.; Bartusch, H. Transient DEM-CFD simulation of solid and fluid flow in a three dimensional blast furnace model. *Powder Technol.* **2018**, *334*, 53–64. [CrossRef]
20. Brännbacka, J.; Saxén, H. Model analysis of the operation of the blast furnace hearth with a sitting and floating dead man. *ISIJ Int.* **2003**, *43*, 1519–1527. [CrossRef]
21. Nightingale, R.J.; Tanzil, F.W.B.U. A novel approach in the estimation of blast furnace hearth voidage. *Iron Steelmaker* **1997**, *24*, 35.
22. Swartling, M.; Sundelin, B.; Tilliander, A.; Jönsson, P.G. Heat transfer modelling of a blast furnace hearth. *Steel Res. Int.* **2010**, *81*, 186–196. [CrossRef]
23. Nightingale, R.J. The Development and Application of Hearth Voidage Estimation and Deadman Cleanliness Index for the Control of Blast Furnace Hearth Operation. Ph.D. Thesis, University of Wollongong, Wollongong, Australia, 2000.
24. Raipala, K. On Hearth Phenomena and Hot Metal Carbon Content in Blast Furnace. Ph.D. Thesis, Helsinki University of Technology, Helsinki, Finland, 2003.
25. Pan, Y.; Zuo, H.; Wang, J.; Xue, Q.; Wang, G.; She, X. Review on improving gas permeability of blast furnace. *J. Iron Steel Res. Int.* **2020**, *27*, 121–131. [CrossRef]
26. Zhang, L.; Zhang, J.; Hu, X.; Liu, Z.; Ma, H.; Jiao, K. Behavior of liquid passing through deadman: Influence of slag/iron ratio and unburned pulverized coal. *J. Iron Steel Res. Int.* **2021**, *28*, 1095–1104. [CrossRef]
27. Shao, L.; Zhang, C.; Qu, Y.; Saxén, H.; Zou, Z. Numerical simulation of hot metal carbonization by dead-man coke in the blast furnace hearth. *Steel Res. Int.* **2020**, *91*, 1900460. [CrossRef]
28. Raipala, K. Deadman and hearth phenomena in the blast furnace. *Scand. J. Metall.* **2000**, *29*, 39–46. [CrossRef]